ADVANCED ENERGY MATERIALS

www.advenergymat.de

# Selective Etching of Nitrogen-Doped Carbon by Steam for Enhanced Electrochemical $CO_2$ Reduction

*Xiaoqi Cui, Zhiyong Pan, Lijuan Zhang, Huisheng Peng, and Gengfeng Zheng**

**Nitrogen-doped carbon structures have recently been demonstrated as a promising candidate for electrocatalytic $CO_2$ reduction, while in the meantime the pyridinic and graphitic nitrogen atoms also present high activities for electroreduction of water. Here, an etching strategy that uses hot water steam to preferentially bind to pyridinic and graphitic nitrogen atoms and subsequently etch them in carbon frameworks is reported. As a result, pyrrolic nitrogen atoms with low water affinity are retained after the steam etching, with a much increased level of among all nitrogen species from 22.1 to 55.9%. The steam-etched nitrogen-doped carbon catalyst enables excellent electrocatalytic $CO_2$ reduction performance but low hydrogen evolution reaction activity, suggesting a new approach for tuning electrocatalyst activity.**

The fast growing utilization of fossil fuels has been leading to a significant increase of $CO_2$ emission in the past several decades, with the $CO_2$ level in the atmosphere has surpassed 400 ppm by 2016.[1] The electrochemical $CO_2$ reduction reaction ($CO_2RR$) in aqueous electrolytes has been regarded as a promising carbon neutral route,[2–4] in which hydrogen evolution reaction (HER) plays as a major competing side reaction. Metal-based electrocatalysts such as Cu, Au, Ag, and Sn have been demonstrated good $CO_2RR$ activities over HER,[5–8] with research focused on tuning catalyst particle size,[7,9–11] morphology,[12,13] defect,[14,15] and grain boundaries.[8,16–18]

Carbon-based materials have been widely used for energy storage and conversion.[19–21] Recently, nitrogen-doped carbon materials have been attracting substantial attention as $CO_2$ electrochemical catalysts, and their catalytic selectivity and activity strongly depend on the nitrogen doping level and dopant types.[22–27] Different nitrogen dopant types and concentrations in carbon materials have generally been achieved by using different precursors as carbon resources[25] or adjusting carbonization temperature during synthesis.[28–30] For instance, Ajayan and coworkers synthesized nitrogen-doped carbon nanotubes and found out that pyridinic and graphitic nitrogen atoms show high activities for the electroreduction of both $CO_2$ and $H_2O$, while pyrrolic nitrogen only presents good activity for $CO_2$ reduction but much more sluggish toward HER.[26] Although Wentrup and Winter have previously shown that pyridinic nitrogen can be converted into pyrrolic nitrogen by thermal nitrene–nitrene rearrangements,[31] the postgrowth tuning of nitrogen dopant structures has seldom been reported.[32]

As different nitrogen types such as pyridinic, pyrrolic, and graphitic N have clearly different affinity to water molecules,[26] we hypothesize that one might use hot steam etching to tune the ratio of different nitrogen atoms in carbon frameworks. Steam etching is a traditional method to etch carbon to form carbon monoxide. Due to their stronger water affinity, the pyridinic and graphitic nitrogen atoms are more prone to induce the steam etching of its adjacent carbon atoms, which may break its original planar structure to a nonplanar one. Thus, the steam-etched nitrogen-doped carbon frameworks may exhibit an increased pyrrolic N level and subsequently a much enhanced selectivity of $CO_2$ electroreduction.

In this work, we have designed a steam etching strategy to tune the nitrogen dopant types and levels, for superior capability of electrochemical $CO_2RR$. **Figure 1**a shows the fabrication steps of nitrogen-doped carbon-wrapped carbon nanotubes (CN-CNTs) and transformation of nitrogen type via steam etching. $H_2O$ molecules prefer to bind to carbon atoms around graphitic and pyridinic nitrogen and lead to selective etching. After the steam etching, pyrrolic nitrogen becomes the majority nitrogen form in the obtained nitrogen-doped carbon network (designed as CN-H-CNT), with a much increased level from 22.1 to 55.9% among the total N species. This steam-etched CN-H-CNT catalyst enables excellent $CO_2RR$ performance but low HER activity (Figure 1b), with a high $CO_2RR$ selectivity (≈88%) toward the formation of CO under −0.5 V versus reversible hydrogen electrode (RHE).

The optical photograph (Figure S1, Supporting Information) and scanning electron microscopy images of the pure CNT (**Figure 2**a), steam-treated CNT (H-CNT, Figure 2b), nitrogen-doped CNT (CN-CNT, Figure 2c), and steam-treated nitrogen-doped CNT (CN-H-CNT, Figure 2d) do not show significant difference in their appearance or surface morphologies (see Methods in the Supporting Information). Transmission

X. Cui, Dr. L. Zhang, Prof. G. Zheng
Laboratory of Advanced Materials
Department of Chemistry, Collaborative Innovation Center of Chemistry for Energy Materials
Fudan University
200438 Shanghai, China
E-mail: gfzheng@fudan.edu.cn

Z. Pan, Prof. H. Peng
State Key Laboratory of Molecular Engineering of Polymers
Department of Macromolecular Science and Laboratory of Advanced Materials
Fudan University
200438 Shanghai, China

The ORCID identification number(s) for the author(s) of this article can be found under https://doi.org/10.1002/aenm.201701456.

**DOI: 10.1002/aenm.201701456**

 

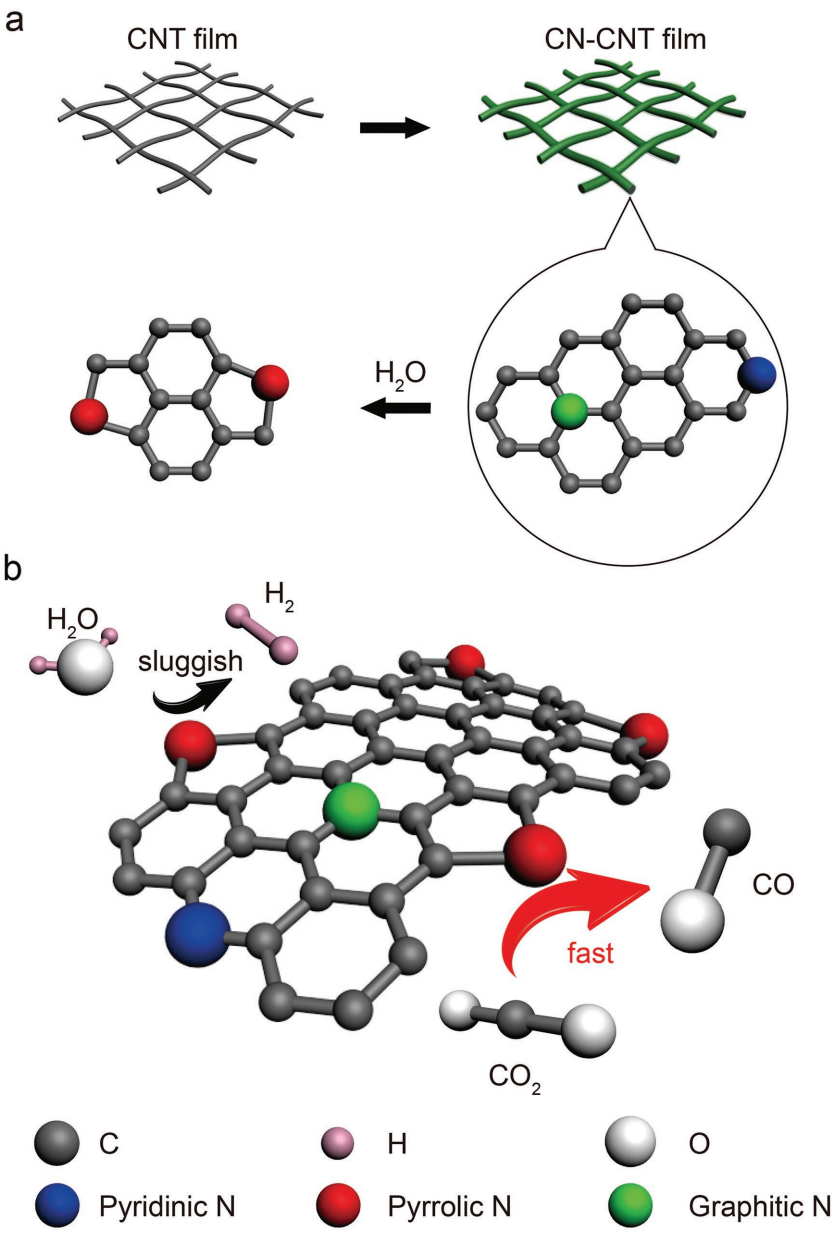


**Figure 1.** Schematic illustration of the synthesis of CH-H-CNTs and catalytic ability for $CO_2$ and $H_2O$ transformation. a) Fabrication of CN-H-CNTs and transformation of nitrogen types by $H_2O$ (steam) etching. b) $CO_2$ electrochemical reduction capability of CN-H-CNTs and passivation for HER reaction.

electron microscope (TEM) images reveal that the diameters of pristine and stream-treated CNTs are around 10 nm (insets in Figure 2a,b). After the growth of nitrogen-doped carbon, the sizes increase to 30–40 nm (insets in Figure 2c,d). The Raman spectra of four CNT materials show characteristic D and G bands at around 1400 and 1600 $cm^{-1}$ (Figure 2e), associated with disordered $sp^2$ hybridized carbon and crystalline graphitic carbon, respectively.[25] The second-order G bands (G′, 2686 $cm^{-1}$) of CN-CNTs and CN-H-CNTs are much weaker than CNTs and H-CNTs, as the graphitic CNT cores are covered by N-doped carbon with large amount of defects. The intensity ratio between these D and G bands ($I_D/I_G$) is 0.54 for the CN-CNTs, higher than that of the pristine CNTs (0.19), indicating the introduction of defects by N doping. After steam etching, the $I_D/I_G$ ratios of H-CNT and CN-H-CNTs are increased to 0.53 and 0.63, respectively, suggesting that the steam etching creates more defects.

X-ray photoelectron spectroscopy (XPS) was carried out to investigate the chemical states of the nitrogen dopants (Figure S2, Supporting Information, for O 1s and C 1s). The high-resolution N 1s spectra of CN-CNTs and CN-H-CNTs are displayed in **Figure 3**a,b, respectively. Both spectra can be deconvoluted into four subpeaks at around 398.2, 400.5, 401.3 and 403.4 eV, corresponding to the four nitrogen configurations, that is, pyridinic, pyrrolic, graphitic, and oxidized N in the carbon network, respectively.[32] The nitrogen contents before and after steam etching are summarized in Figure 3c. For CN-CNTs, the atomic percentages of pyridinic, pyrrolic, graphitic, and oxidized N among all the nitrogen species are 19.2, 22.1, 40.5 and 18.2%, respectively. For CN-H-CNTs, the percentages of pyridinic, graphitic, and oxidized N atoms decrease to 9.8, 24.9 and 9.4%, respectively, while pyrrolic N increases substantially from 22.1 to 55.9%, indicating its predominant existence in CN-H-CNTs after the steam etching. The total nitrogen percentages in CN-CNTs and CN-H-CNTs are 6.3 and 6.9% before and after the steam etching, respectively (Figure 3d), suggesting the similar etching rates of nitrogen and carbon atoms. Taken together, it can be concluded that different etching selectivity is clearly associated with the nitrogen types in the carbon frameworks, in which pyrrolic N remains as the most stable structure upon steam etching.

The electrochemical $CO_2RR$ was then evaluated for these catalysts in a three-electrode format in a $CO_2$-saturated electrolyte (see Methods in the Supporting Information). Cyclic voltammetry (CV) curves show that CN-H-CNTs have the lowest onset potential of −0.2 V versus RHE, and the largest current density (**Figure 4**a), suggesting its highest electrocatalytic activity. The electrochemically active surface areas (ECSAs) of these three catalysts were evaluated by electrochemical double-layer capacitance ($C_{dl}$). The electrochemical double-layer capacitances of the CN-H-CNTs, CN-CNTs, and H-CNTs are calculated as 5.34, 3.11 and 0.49 μF $cm^{-2}$, respectively (Figure S3, Supporting Information). The highest electrochemical capacitance of CN-H-CNT indicates its largest effective electrochemical area for electrocatalysis among these samples.

The faradic efficiencies (FE) of these catalysts for CO formation ($FE_{CO}$), HER ($FE_{H2}$), and methane formation ($FE_{CH4}$) were

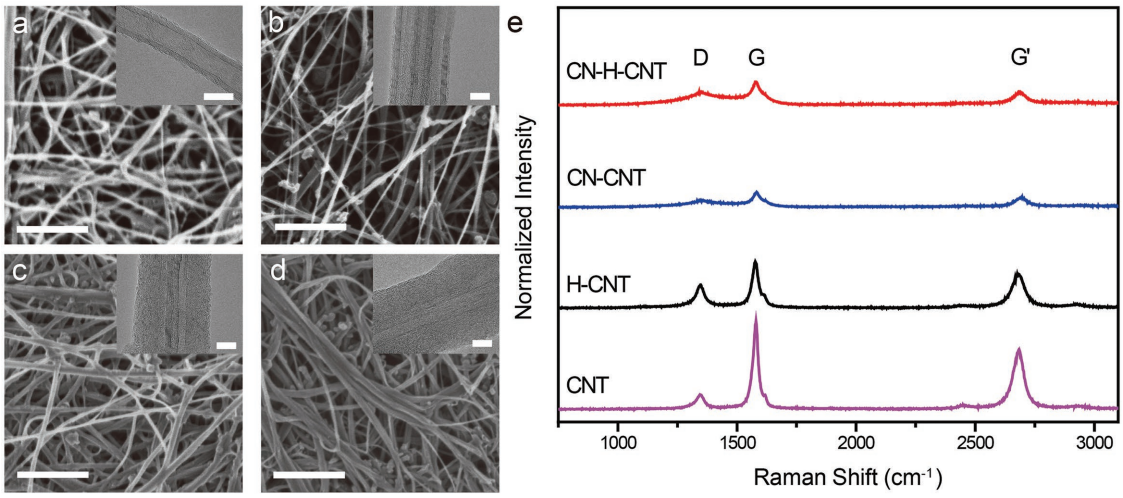


**Figure 2.** SEM images of a) CNTs, b) H-CNTs, c) CN-CNTs, and d) CN-H-CNTs. Scale bars in (a)–(d): 500 nm. Insets: corresponding TEM images for each sample. Scale bars in insets: 10 nm. e) Raman spectra of CNTs, H-CNTs, CN-CNTs, and CN-H-CNTs.

measured by in-line gas chromatography. In all three cases, the FE values of these gas products were added to over 95%, and no other liquid products were detected. For CN-H-CNTs (Figure 4b), the FE of CO formation ($FE_{CO}$) increases from –0.3 to –0.5 V versus RHE and reaches maximum (≈88%) at –0.5 V, with FE of water reduction ($FE_{H2}$) synchronically drops in the same voltage range to <≈10% at –0.5 V. As for CN-CNTs (Figure 4c), the peak of $FE_{CO}$ accounts for ≈60% of current density at –0.6 V versus RHE, accompanying by the significantly higher $FE_{H2}$ to ≈40%. As a control, H-CNTs show almost no

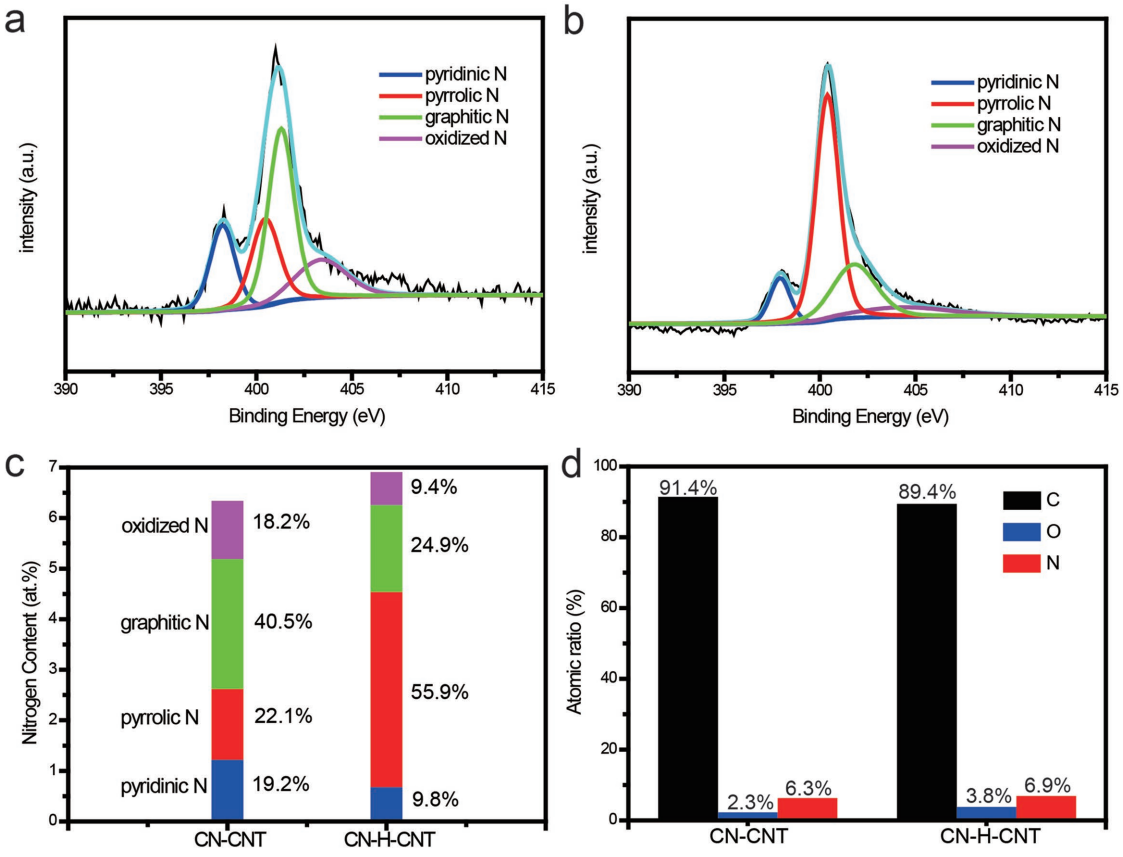


**Figure 3.** XPS spectra and atomic distributions of CN-CNTs and CN-H-CNTs. Representative XPS spectra of N 1s for a) CN-CNTs and b) CN-H-CNTs. Summary of N atomic contents and total atomic concentrations in c) CN-CNTs and d) CN-H-CNTs.

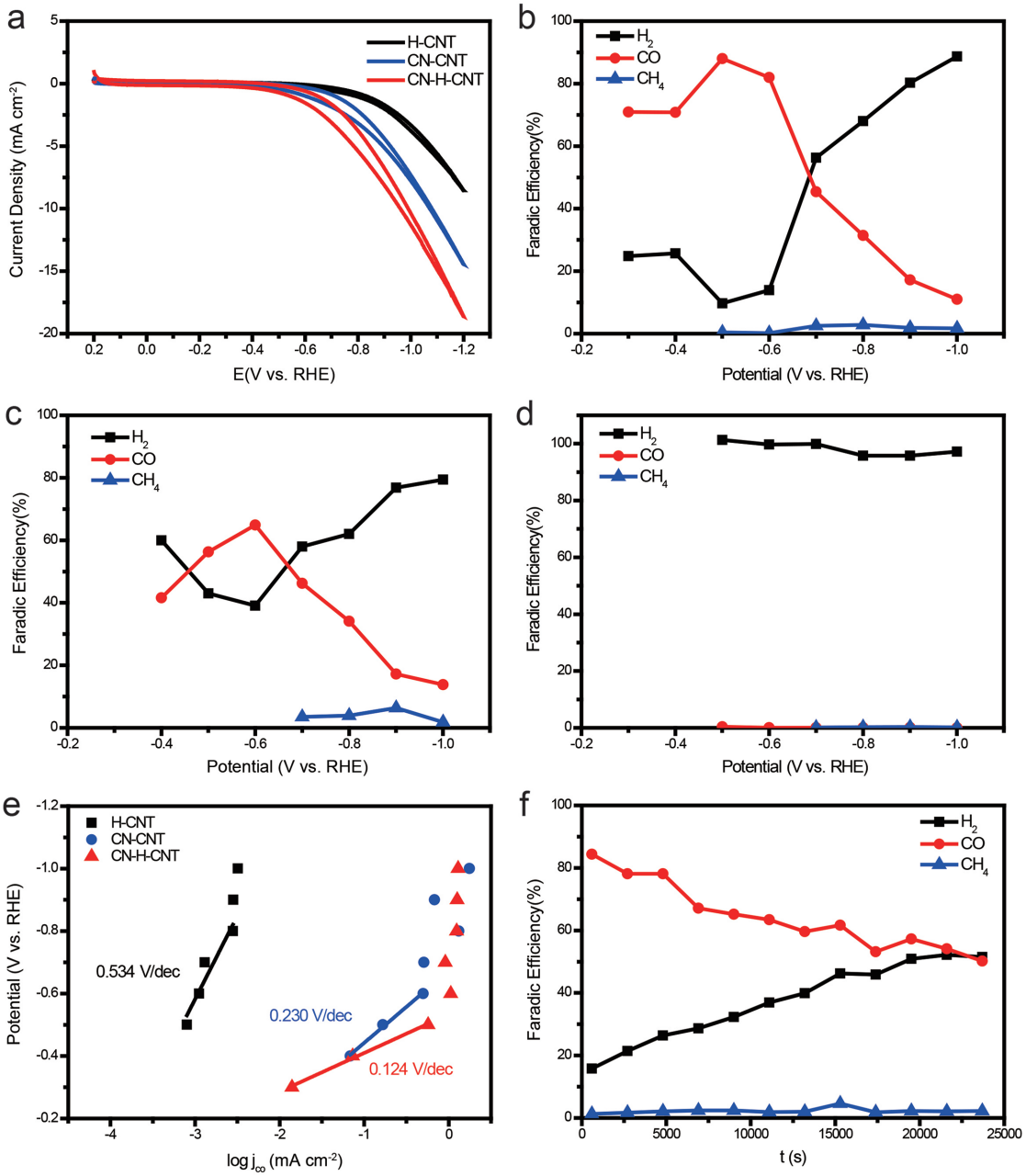


**Figure 4.** Electrochemical $CO_2$ reduction performance. a) CV curves for CN-H-CNTs, CN-CNTs, and H-CNTs in $CO_2$-saturated 0.1 M $KHCO_3$ electrolyte. The scan rate was 20 mV $s^{-1}$. Faradaic efficiency for CO, $H_2$, and $CH_4$ versus potential on b) CN-H-CNTs, c) CN-CNTs, and d) H-CNTs, respectively. e) Tafel plots for CO formation on CN-H-CNTs, CN-CNTs, and H-CNTs. f) Stability of faradaic efficiency of CN-H-CNTs for $CO_2$ reduction at the potentiostatic mode of –0.5 V versus RHE.

activity for $CO_2$RR but predominantly HER (Figure 4d), due to the lack of nitrogen dopants. As suggested in Ajayan's theoretical calculations, pyrrolic N provides excellent capabilities for $CO_2$ reduction and HER suppression. To verify the HER suppression ability of pyrrolic N, CV tests of CN-H-CNTs and CN-CNTs were carried out in an Ar-saturated electrolyte (Figure S4, Supporting Information). The onset potential of CN-H-CNTs was 83 mV more negative than that of CN-CNTs, indicating the requirement of more energy for HER to take place on the surface of CN-H-CNTs. Thus, CN-H-CNTs have the highest pyrrolic N concentration, and subsequently the best selectivity and activity toward $CO_2$ reduction among three catalysts.

The reaction kinetics for the CO formation was analyzed by the Tafel slopes of the logarithm of CO partial current density (i.e., log $j_{CO}$), as shown in Figure 4e. The measured Tafel slope for CN-H-CNTs is 0.124 V $dec^{-1}$, lower than that of CN-CNTs (0.230 V $dec^{-1}$) and H-CNTs (0.534 V $dec^{-1}$). These results demonstrate that CN-H-CNTs have more rapid kinetic activities.[15] For CN-H-CNTs, the Tafel slope is close to the value of 0.118 V $dec^{-1}$, suggesting that the rate-determining

step of $CO_2$RR is the acquisition of an electron by $CO_2$ to form a surface adsorbed $CO_2^{\bullet-}$ intermediate.[33–36] The stability measurement for CN-H-CNTs was carried out by the potentiostatic method at −0.5 V versus RHE for 24 000 s (Figure S5, Supporting Information). The current density shows a quick drop at the beginning and then remains almost stable after 1200 s. This initial drop can be attributed to the fast consumption of $CO_2$ near the electrode, similar to previous reports.[33,35] Nonetheless, the faradic efficiency of $CO_2$ reduction still presents a good retention, with $FE_{CO}$ changing from 84.4 to 50.2%) after the 24 000 s period (Figure 4f), suggesting the good electrocatalytic stability of the CN-H-CNTs. The stability measurement for CN-CNTs was also carried out for comparison (Figure S6, Supporting Information), which shows that the steam treatment can slightly improve the catalytic stability of faradic efficiency. To verify the reason of deactivation, we investigated the chemical states of nitrogen dopants after 25 000 s stability test (Figure S7a, Supporting Information). The atomic percentages of pyridinic, pyrrolic, graphitic, and oxidized N were 11.4, 51.9, 30.2, and 6.5%, respectively (Figure S7b, Supporting Information), no obvious differences compared with the original one. However, the atomic concentration of N dropped from 6.9 to 4.0% (Figure S7c, Supporting Information), which could be the cause of deactivation.

In conclusion, we have developed a unique steam-etching approach for tuning the configurations of nitrogen dopants in carbon frameworks. The carbon atoms around pyridinic and graphitic N are more prone to be etched by steam due to their stronger binding capability to water molecules, thus resulting in a much enhanced pyrrolic N dopant percentage. The obtained CN-H-CNT catalyst shows an excellent $CO_2$ reduction catalytic activity and HER suppression, with a maximum faradaic efficiency of ≈88% toward the formation of CO under −0.5 V versus RHE. This work suggests a new strategy for adjusting intrinsic configuration of nitrogen-doped carbon materials and developing efficient and robust catalysts for carbon cycle.

## Supporting Information

Supporting Information is available from the Wiley Online Library or from the author.

## Acknowledgements

X.C. and Z.P. contributed equally to this work. The authors thank the following funding agencies for supporting this work: the National Key Research and Development Program of China (2017YFA0206901, 2017YFA0206900), the Natural Science Foundation of China (21473038, 21471034), the Science and Technology Commission of Shanghai Municipality (14JC1490500), the Program for Professor of Special Appointment (Eastern Scholar) at Shanghai Institutions of Higher Learning, and the Collaborative Innovation Center of Chemistry for Energy Materials (2011-iChem).

## Conflict of Interest

The authors declare no conflict of interest.

## Keywords

$CO_2$ reduction, faradaic efficiency, nitrogen doping, pyrrolic, steam etching

Received: May 27, 2017
Revised: July 5, 2017
Published online: September 1, 2017

[1] D. D. Zhu, J. L. Liu, S. Z. Qiao, *Adv. Mater.* **2016**, *28*, 3423.
[2] N. S. Lewis, D. G. Nocera, *Proc. Natl. Acad. Sci. USA* **2006**, *103*, 15729.
[3] S. N. Habisreutinger, L. Schmidt-Mende, J. K. Stolarczyk, *Angew. Chem. Int. Ed.* **2013**, *52*, 7372.
[4] H. Mistry, A. S. Varela, S. Kühl, P. Strasser, B. R. Cuenya, *Nat. Rev. Mater.* **2016**, *1*, 16009.
[5] R. Kas, K. K. Hummadi, R. Kortlever, P. De Wit, A. Milbrat, M. W. Luiten-Olieman, N. E. Benes, M. T. Koper, G. Mul, *Nat. Commun.* **2016**, *7*, 10748.
[6] M. Liu, Y. Pang, B. Zhang, P. De Luna, O. Voznyy, J. Xu, X. Zheng, C. T. Dinh, F. Fan, C. Cao, F. P. Arquer, T. S. Safaei, A. Mepham, A. Klinkovva, E. Kumacheva, T. Filleter, D. Sinton, S. O. Kelley, E. H. Sargent, *Nature* **2016**, *537*, 382.
[7] C. Kim, H. S. Jeon, T. Eom, M. S. Jee, H. Kim, C. M. Friend, B. K. Min, Y. J. Hwang, *J. Am. Chem. Soc.* **2015**, *137*, 13844.
[8] B. Kumar, V. Atla, J. P. Brian, S. Kumari, T. Q. Nguyen, M. Sunkara, J. M. Spurgeon, *Angew. Chem. Int. Ed.* **2017**, *56*, 3645.
[9] A. Loiudice, P. Lobaccaro, E. A. Kamali, T. Thao, B. H. Huang, J. W. Ager, R. Buonsanti, *Angew. Chem. Int. Ed.* **2016**, *55*, 5789.
[10] R. Reske, H. Mistry, F. Behafarid, B. R. Cuenya, P. Strasser, *J. Am. Chem. Soc.* **2014**, *136*, 6978.
[11] D. Gao, H. Zhou, J. Wang, S. Miao, F. Yang, G. Wang, J. Wang, X. Bao, *J. Am. Chem. Soc.* **2015**, *137*, 4288.
[12] A. S. Hall, Y. Yoon, A. Wuttig, Y. Surendranath, *J. Am. Chem. Soc.* **2015**, *137*, 14834.
[13] Y. Yoon, A. S. Hall, Y. Surendranath, *Angew. Chem. Int. Ed.* **2016**, *128*, 15508.
[14] S. Gao, X. Jiao, Z. Sun, W. Zhang, Y. Sun, C. Wang, Q. Hu, X. Zu, F. Yang, S. Yang, L. Lang, J. Wu, Y. Xie, *Angew. Chem. Int. Ed.* **2016**, *55*, 698.
[15] S. Gao, Y. Lin, X. Jiao, Y. Sun, Q. Luo, W. Zhang, D. Li, J. Yang, Y. Xie, *Nature* **2016**, *529*, 68.
[16] A. D. Handoko, C. W. Ong, Y. Huang, Z. G. Lee, L. Lin, G. B. Panetti, B. S. Yeo, *J. Phys. Chem. C* **2016**, *120*, 20058.
[17] K.-S. Kim, W. J. Kim, H.-K. Lim, E. K. Lee, H. Kim, *ACS Catal.* **2016**, *6*, 4443.
[18] X. Feng, K. Jiang, S. Fan, M. W. Kanan, *J. Am. Chem. Soc.* **2015**, *137*, 4606.
[19] J. Wang, W. Cui, Q. Liu, Z. Xing, A. M. Asiri, X. Sun, *Adv. Mater.* **2016**, *28*, 215.
[20] R. Lv, T. Cui, M. S. Jun, Q. Zhang, A. Cao, D. S. Su, Z. Zhang, S. H. Yoon, J. Miyawaki, I. Mochida, F. Kang, *Adv. Funct. Mater.* **2011**, *21*, 999.
[21] H. Ye, L. Wang, S. Deng, X. Zeng, K. Nie, P. N. Duchesne, B. Wang, S. Liu, J. Zhou, F. Zhao, N. Han, P. Zhang, J. Zhong, X. Sun, Y. Li, J. Lu, *Adv. Energy Mater.* **2017**, *7*, 1601602.
[22] B. Kumar, M. Asadi, D. Pisasale, S. Sinha-Ray, B. A. Rosen, R. Haasch, J. Abiade, A. L. Yarin, A. Salehi-Khojin, *Nat. Commun.* **2013**, *4*, 2819.
[23] S. Zhang, P. Kang, S. Ubnoske, M. K. Brennaman, N. Song, R. L. House, J. T. Glass, T. J. Meyer, *J. Am. Chem. Soc.* **2014**, *136*, 7845.

 

[24] J. Wu, R. M. Yadav, M. Liu, P. P. Sharma, C. S. Tiwary, L. Ma, X. Zou, X.-D. Zhou, B. I. Yakobson, J. Lou, P. M. Ajayan, *ACS Nano* **2015**, *9*, 5364.
[25] P. P. Sharma, J. Wu, R. M. Yadav, M. Liu, C. J. Wright, C. S. Tiwary, B. I. Yakobson, J. Lou, P. M. Ajayan, X. D. Zhou, *Angew. Chem. Int. Ed.* **2015**, *127*, 13905.
[26] J. Wu, M. Liu, P. P. Sharma, R. M. Yadav, L. Ma, Y. Yang, X. Zou, X.-D. Zhou, R. Vajtai, B. I. Yakobson, J. Lou, P. M. Ajayan, *Nano Lett.* **2015**, *16*, 466.
[27] J. Wu, S. Ma, J. Sun, J. I. Gold, C. Tiwary, B. Kim, L. Zhu, N. Chopra, I. N. Odeh, R. Vajtai, A. Z. Yu, R. Luo, J. Lou, G. Ding, P. J. Kenis, P. M. Ajayan, *Nat. Commun.* **2016**, *7*, 13869.
[28] M. A. Wójtowicz, J. R. Pels, J. A. Moulijn, *Fuel* **1995**, *74*, 507.
[29] L. Lai, J. R. Potts, D. Zhan, L. Wang, C. K. Poh, C. Tang, H. Gong, Z. Shen, J. Lin, R. S. Ruoff, *Energy Environ. Sci.* **2012**, *5*, 7936.
[30] D. Geng, Y. Chen, Y. Chen, Y. Li, R. Li, X. Sun, S. Ye, S. Knights, *Energy Environ. Sci.* **2011**, *4*, 760.
[31] C. Wentrup, H. W. Winter, *J. Am. Chem. Soc.* **1980**, *102*, 6159.
[32] D. Guo, R. Shibuya, C. Akiba, S. Saji, T. Kondo, J. Nakamura, *Science* **2016**, *351*, 361.
[33] Y. Chen, C. W. Li, M. W. Kanan, *J. Am. Chem. Soc.* **2012**, *134*, 19969.
[34] C. W. Li, J. Ciston, M. W. Kanan, *Nature* **2014**, *508*, 504.
[35] C. W. Li, M. W. Kanan, *J. Am. Chem. Soc.* **2012**, *134*, 7231.
[36] Y. Chen, M. W. Kanan, *J. Am. Chem. Soc.* **2012**, *134*, 1986.